Quantitative trait locus mapping of osmotic stress response in the wheat pathogen *Zymoseptoria tritici*

Authors:

Jessica Stapley and Bruce A. McDonald

Plant Pathology Group, Institute of Integrative Biology, ETH Zurich, 8092 Zürich, Switzerland

Corresponding author: Jessica Stapley, Jessica.stapley@usys.ethz.ch

Abstract

Osmotic stress is a ubiquitous and potent stress for all living organisms. Fungal molecular responses to salt stress in well studied model yeast species highlighted the importance of the conserved HOG MAP kinase pathway. However, fewer studies have investigated the genetic basis of salt tolerance in filamentous fungi. The main aim of this study was to identify regions of the genome associated with tolerance to potassium chloride in the wheat pathogen *Zymoseptoria tritici.* A secondary aim was to identify candidate genes affecting salt tolerance within the most promising chromosomal regions. We achieved these aims with a QTL mapping study using offspring from two crosses grown in vitro in the presence or absence of osmotic stress imposed by 0.75M KCl. We identified significant QTLs for most of the traits in both crosses. Several QTLs overlapped with QTLs identified in earlier studies for other traits and some QTLs explained trait variation in both the control and salt stress environments. A significant QTL on chromosome 3 explained variation in colony radius at 8 days post inoculation (dpi) in the KCl environment as well as KCl-tolerance affecting colony radius at 8 dpi. The QTL peak had a high LOD and encompassed an interval containing only 36 genes. Six of these genes present promising candidates for functional analyses.

Keywords:
Salt stress; plant pathogen; fungi; *Mycosphaerella graminicola*, QTL

1. Introduction

Osmotic stress is a common and potent environmental stress that can limit growth and reproduction in many organisms. At the cellular level osmotic stress results in changes to the movement of water into or out of the cell through osmosis. To counteract osmotic stress, organisms need to accumulate compatible solutes (e.g. glycerol, erythritol, arabitol, mannitol and trehalose) – that can balance osmosis and provide turgor pressure (Araújo et al., 2020; Kogej et al., 2007). In fungal pathogens of plants, the pathogen may be exposed to a relatively high salt concentration (0.5M) within the plant (see Araújo et al., 2020) as well as experience changes in salt and osmolyte concentrations as plant tissues degrade (Jacob et al., 2015). The genes and pathways involved in responding to the resulting osmotic stresses may also affect plant-pathogen interactions and virulence. For example, turgor pressure which is mediated by changes in vacuole size and number is important in both plant tissue penetration and response to osmotic stress (Richards et al., 2010). Voltage-gated chloride channels, which are involved in regulation of cell volume, also influence virulence in fungal pathogens of both plants and humans (Cañero and Roncero, 2008; Zhu and Williamson, 2003). Knowledge of the genetic basis of osmotic sensitivity in plant pathogens can thus provide important insights into the genetic basis of environmental stress responses as well as disease development.

The immediate effects of osmotic stress in fungi include stalled growth, changes in the recruitment of water, collapse of the cytoskeleton, altered plasma membranes and a reduction in glycerol transport (Duran et al., 2010; Hohmann, 2002). Longer-term adaptation to osmotic stress involves modifications of metabolism, plasma membranes, cell wall thickness and cell wall melanisation, as well as an accumulation of mycosporines (Hohmann, 2002; Kogej et al., 2007). Osmotic stress is also likely to activate many genes and pathways involved in the ‘general stress response’. For example, up to 10% of the genes that were differentially expressed under different individual stressors were shared across these different treatments (Hohmann, 2002).

Although the key salt stress response pathways and genes have been identified and well characterized in model yeasts, studies in filamentous fungi could provide novel insights into the genes involved in responding to osmotic stress. The HOG pathway is an osmoresponsive

67 system and one of the most well-understood Mitogen-activated protein (MAP) kinase
68 pathways (Hohmann, 2002). In yeast, two genes are central components of this pathway –
69 Pbs2 and Hog1p kinase. In plant pathogens, HOG signalling appears more complex than in
70 yeast, although it is still poorly understood (Jacob et al., 2015). Several filamentous
71 pathogenic fungi (including our model *Zymoseptoria tritici*) have multiple (up to 17) histidine
72 kinases, whereas *S. cerevisiae* has only one (Sln1p) (Jacob et al., 2015). Several studies have
73 identified transcription factors involved in regulating fungal response to salt stress, as well
74 as other stressors - including temperature and fungicide stress. For example, in *Aspergillus*
75 *oryzae*, GATA transcription factors (TFs) were shown to be important in responding to salt
76 and temperature stress (Jiang et al., 2021). In the causal agent of Fusarium head blight
77 (*Fusarium graminearum*), the Nutrient and stress factor 1 (*NSf1*) C_2H_2 zinc fingers protein
78 plays an important role in salt stress response, sexual-asexual reproduction, vegetative
79 growth, fungicide sensitivity and pathogenicity (Shi et al., 2021), and a Zn(2)-C6 fungal-type
80 DNA-binding TF (Fss1) is required for sodium and lithium tolerance (Son et al., 2015). Cell
81 wall melanisation also appears to confer benefits for osmotic stress tolerance. For example,
82 in halotolerant fungi cell wall melanisation helps to maintain high concentrations of glycerol
83 and contain the resulting turgor pressure by strengthening and preventing leakage through
84 the cell wall (Kogej et al., 2007). These examples coming from a relatively small number of
85 fungal species demonstrate how the molecular mechanisms of salt response can vary across
86 taxa and illustrate that additional work is needed to understand how fungi adapt to salt
87 stress.
88
89 To improve our understanding of osmotic stress response in fungi we performed a
90 quantitative trait loci (QTL) mapping study using the wheat pathogen *Z. tritici* growing under
91 salt stress. QTL studies have been instrumental in finding candidate genes for multiple traits
92 in this widespread and damaging wheat pathogen, including melanisation (Lendenmann et
93 al., 2014), fungicide sensitivity (Lendenmann et al., 2015), morphological switching
94 (Francisco et al., 2022) and oxidative stress (Zhong et al., 2021), and enabled the cloning and
95 functional validation of genes affecting virulence (Zhong et al., 2017; Meile et al. 2018),
96 melanisation (Krishnan et al. 2018), and morphological switching (Francisco et al., 2022).
97 QTL mapping identifies genomic regions that explain variation in a trait and that are likely to
98 harbour genes responsible for creating variation in the trait. The aim of this study was to

99 identify large effect loci associated with tolerance to salt stress in *Z. tritici* and identify
100 plausible candidate genes within the most promising QTL intervals.
101
102 **2. Methods**
103 **2.1. QTL mapping crosses**
104 Parent and progeny isolates used in this study are from two crosses that were described
105 previously (Lendenmann et al., 2014). The crosses were made by coinfecting wheat leaves
106 with the parent strains, with the resulting ascospores collected from infected leaves and
107 grown in vitro. One cross was between ST99CH1A5 and ST99CH1E4 (herein referred to as
108 1A5 and 1E4 respectively) and the other was between ST99CH3D7 and ST99CH3D1 (herein
109 referred to as 3D7 and 3D1 respectively).
110
111 **2.2. Genotyping**
112 SNP genotype data for the progeny were obtained from a RAD sequence dataset that was
113 previously produced in our lab (first described in (Lendenmann et al., 2014). In brief, the
114 genome was cut using the restriction enzyme *Pst*I and the libraries were sequenced on an
115 Illumina HiSeq2000 with paired-end sequencing. Complete genome sequences of the
116 parental strains (Croll et al., 2013)(NCBI Biosample: SRS383146 (ST99CH3D1), SRS383147
117 (ST99CH3D7), SRS383142 (ST99CH1A5), and SRS383143 (ST99CH1E4)) were used to SNP
118 genotype the parents and offspring.
119
120 RADseq processing and variant discovery is described in detail at
121 https://github.com/jessstapley/QTL-mapping-Z.-tritici. In brief, RADseq reads were trimmed
122 of adaptors and low-quality sequence using trimmomatic (v0.35). The RADseq reads were
123 mapped to a reference genome using bwa mem (v0.7.17). Reads from progeny of the
124 3D7x3D1 cross were mapped to the 3D7 reference genome and progeny from the 1A5x1E4
125 cross were mapped to the 1A5 reference genome. Variant calling was done using the GATK
126 Germline Short Variant Discovery pipeline, following their Best Practice recommendations
127 (https://gatk.broadinstitute.org/hc/en-us/sections/360007226651-Best-Practices-
128 Workflows). After this we applied the following filters: only biallelic SNPs, parents had
129 alternative alleles, <50% missing genotypes per marker, <50% missing genotypes per
130 individual, mean read depth >3 and <30, depth quality (QD)>5, mapping quality >40, minor

131 allele frequency >0.02 and <0.80, and SNPs in regions where the SNP density is >3 in 10bp
132 were removed.
133
134 **2.3. Generating linkage maps**
135 Linkage maps were made using R (R Core Team, 2020), R Studio (RStudio Team, 2020) and
136 the R package qtl (v1.48-1 (Broman et al., 2003)). As the order and base pair positions of the
137 markers were known from the reference genomes, we only needed to calculate the
138 recombination distance between markers to create the linkage map. Before map
139 construction, we removed putative clones. To do this we calculated genetic similarity using
140 the 'comparegeno' function and removed individuals with >99% shared genotypes (83
141 progeny were removed from the 1A5x1E4 cross, 74 progeny were removed from the
142 3D7x3D1 cross). The linkage map was constructed for each chromosome separately using
143 the 'estimatemap' function with method 'morgan'. Then we performed multiple rounds of
144 cleaning to remove error-prone markers that caused map inflation. First, we removed
145 markers that had an estimated recombination distance above the 99.9% quantile. Then
146 recombination rate was estimated again and we inspected the maps. In regions of the map
147 where there was evidence of map inflation and spurious double recombination events, we
148 visualised these regions in an Integrated Genome Viewer (IGV, https://igv.org) to look at the
149 mapping alignments. Markers were removed from regions with poor alignments and
150 evidence of mismapping. A summary of the two linkage maps is provided in Supplementary
151 Material S1 and the complete maps are available at (https://github.com/jessstapley/QTL-
152 mapping-Z.-tritici). After applying all these filters, the average marker spacing was 1217 bp
153 (0.19 cM) and 529 bp (0.14 cM) for the 1A5x1E4 and 3D7x3D1 crosses, respectively.
154
155 **2.4. Phenotyping**
156 We compared colony growth and melanisation in a control environment and in the
157 presence of potassium chloride (KCl) to simulate a salt stress environment. Potassium
158 chloride (KCl) has been used extensively in the study of stress response in fungi because it is
159 environmentally ubiquitous and lacks the toxic effects of Na^+ (Araújo et al., 2020; Hohmann,
160 2002). Only non-clonal offspring strains were phenotyped (for 1A5x1E4 n= 259 strains; for
161 3D7x3D1 n=265 strains). The basic protocols for isolate recovery from -80^{0}C storage, growth
162 in vitro and the measurements of colony size and colony melanisation were described

163 previously (Zhong et al., 2021). In brief, Petri dishes containing Difco potato dextrose agar
164 (PDA) were inoculated with 200µl of a spore solution (concentration 200 spores/ml) and
165 grown at 18^0C for 8 and 12 days. In the salt stress environment, a sterile potassium chloride
166 solution was added to the cooled and sterilized PDA to make a final concentration of 0.75M.
167 Three replicates were grown in both the control and salt (KCl) environments.
168
169 Two traits were measured; colony area and colony grey value, using automated image
170 analysis as described previously (Lendenmann et al., 2014; Zhong et al., 2021). Grey value
171 was measured on a scale of 0-255, where darker, more melanised colonies have lower
172 values (0 = black, 255 = white). Mean colony area and grey value were calculated from
173 measurements of multiple colonies on each plate and then the mean was calculated across
174 the three replicate plates to obtain a final mean colony area and mean grey value for each
175 strain in the two environments. Colony area was converted to a radial size measure by
176 dividing by π and taking the square root of this value. Measurements were taken at 8- and
177 12-days post inoculation (dpi). For the analysis we used three different types of data; time
178 point/age: the colony radius and grey value at 8 and 12 dpi; daily rate measurements: the
179 change in colony radius or grey value between 8-12 dpi (i.e. the difference in colony radius
180 between 8 and 12 dpi/difference in days); and tolerance measurements: the ratio of a
181 measurement (colony radius, grey value, growth rate or melanisation rate) between the KCl
182 environment and the control environment (i.e. radius at 8 dpi in KCl environment/radius at
183 8 dpi in control environment, or growth rate in KCl environment/growth rate in control
184 environment). For the tolerance measurements, values >1 indicate the isolate is more
185 tolerant to KCl (grew faster under salt stress), and values <1 indicate that the isolate is more
186 sensitive to KCl. In total there were 18 traits (Table 1).
187
188 **2.5. QTL mapping**
189 QTL mapping was performed using the R (v 3.6.0) package 'qtl2' (v2_0.24) as described in
190 detail on github (https://github.com/jessstapley/QTL-mapping-Z.-tritici). We scanned the
191 genome for a single QTL per chromosome with the '*scan1*' function using a linear mixed
192 effect model, and we controlled for the relatedness of individuals (i.e. we included a
193 random polygenic effect) by fitting the kinship matrix as a random effect. Models that take
194 into account the genetic covariance between individuals can reduce the false discovery rate

195 in QTL scans and outperform models that do not include this information in the model
196 (Malosetti et al., 2011). The significance threshold for a QTL peak was determined by
197 permutation tests (n=1000) and we calculated a Bayes Credible Interval (95%) to identify the
198 interval size around the QTL peak. We used custom R scripts to extract a list of the genes
199 within the interval from the annotation (gff) files of each reference genome. The putative
200 encoded function of each gene was determined in previous analyses (for 1A5 see
201 (Plissonneau et al., 2018), for 3D7 see (Plissonneau et al., 2016)). The annotations were
202 obtained using Interproscan (https://www.ebi.ac.uk/interpro/) against multiple protein
203 databases and then screened using multiple methods (i.e. signalP
204 https://services.healthtech.dtu.dk/service.php?SignalP-5.0, Phobius
205 https://phobius.sbc.su.se/) to determine if the encoded proteins contained likely signal
206 peptides or secreted domains. The putative effect of a SNP in the coding sequence was
207 determined using SNPeff (http://pcingola.github.io/SnpEff/).
208
209 **2.6. Identifying putative candidate genes in the 3D7x3D1 cross**
210 Genes within a single QTL interval on chromosome 3 were further investigated to identify
211 the most likely candidate genes responsible for the phenotype. We identified the
212 orthologous genes in the 3D1 parent using an analysis performed across the genomes of 19
213 reference strains (Badet et al., 2020). We inspected the alignments in the region of interest
214 in IGV. We also blasted the 3D1 gene sequences (including ±200bp flanking regions) against
215 the 3D7 genome to calculate sequence similarity and identify indels.
216
217 **2.7. RNAseq data analysis**
218 We analysed RNAseq data that was previously created for the four parental strains during
219 infection of the susceptible wheat cultivar Drifter (Palma-Guerrero et al., 2017) as well as
220 cultures grown in vitro on two types of liquid media (yeast sucrose broth (YSB): yeast extract
221 10 g/L and sucrose 10 g/L, pH 6.8; and carbon-depleted minimal medium (MM), pH 5.8
222 (Francisco et al., 2019)). The raw sequence reads were downloaded from the Short Read
223 Archive (SRA, https://www.ncbi.nlm.nih.gov/sra, Bioproject: *invitro* SRP152081, *invivo*
224 SRP077418). RNAseq data processing and analysis is described in detail at github
225 (https://github.com/jessstapley/QTL-mapping-Z.-tritici). In brief, reads were trimmed and
226 then mapped to one of two reference genomes (reads from 3D1 and 3D7 were mapped to

227 the 3D7 reference genome while reads from 1E4 and 1A5 were mapped to the 1A5
228 reference genome). Then the number of reads mapping to each gene was counted using
229 R::Rsubread (Liao et al., 2019) and we tested for differential gene expression between
230 strains, 3D7 versus 3D1 and 1A5 versus 1E4, using R::EdgeR (Robinson et al., 2010).
231
232 **3. Results**
233 **3.1. Effect of KCl on growth and melanisation**
234 A total of 158,480 and 120,059 colonies from the 1A5x1E4 and 3D7x3D1 crosses,
235 respectively, were phenotyped (see Table S1 for details). We used paired Wilcoxon tests to
236 compare mean trait values between the control and KCl treatments (Table S1). In the
237 presence of KCl, colony radius was smaller at 8 and 12 dpi in both crosses, and the growth
238 rate was reduced in the 3D7x3D1 cross, but not in the 1A5x1E4 cross, suggesting that
239 isolates from the 3D7x3D1 cross were more sensitive to KCl. This is consistent with the
240 greater mean KCl-tolerance found in the 1A5x1E4 cross compared to the 3D7x3D1 cross
241 (KCl-tolerance in growth: 3D1 = 1.04 versus 3D7 = 0.96, KCl-tolerance in radius at 8 dpi 3D1
242 = 0.42 versus 3D7 = 0.40, KCl-tolerance in radius at 12 dpi 3D1 = 0.70 versus 3D7 = 0.68). In
243 the KCl environment we observed less melanisation at both time points and a reduced
244 accumulation of melanin over time (melanisation rate) in both crosses (Table S1).
245
246 **3.2. Correlations between traits**
247 All pairwise correlations (Pearson, non-parametric) between independent measurements
248 are provided in Tables S2 and S3. Excluding traits that are statistically or functionally
249 coupled, which includes: correlations between two time points of the same trait (i.e. radius
250 at 8 dpi and 12 dpi in the control), correlations between a rate and the corresponding time
251 point measurements (i.e. grey value at 12 dpi and melanisation rate in the control), or
252 correlations between rates and tolerance measurements, we identified many correlations
253 between independent measurements (Table S2 and S3). Notably, growth rate in the control
254 environment was correlated with growth rate in the KCl environment in both crosses
255 (correlation (1A5x1E4) = 0.63 and correlation (3D7x3D1) = 0.62) – thus isolates that grow
256 faster in a benign environment also grow faster in the presence of salt stress, i.e. they have
257 a higher intrinsic growth rate. Melanisation rates showed a similar trend in 1A5x1E4 -
258 isolates that had higher melanisation rates in the benign environment also had higher

259 melanisation rates under KCl stress (Table S3, correlation = 0.19), but this was not observed
260 in the 3D7x3D1 cross (Table S2, correlation = 0.07).
261
262 We were particularly interested in the relationship between KCl tolerance and melanisation,
263 as melanin can help protect cells from osmotic stress. In both crosses, the mean grey value
264 in the control environment at 12 dpi was negatively correlated with KCl-tolerance affecting
265 growth rate (Tables S2 and S3, 1A5x1E4 correlation = -0.26 and 3D7x3D1 correlation = -
266 0.43), the relationship at 8 dpi was also negative in both crosses, but not significant in the
267 3D7x3D1 cross (Tables S2 and S3, 1A5x1E4 correlation = -0.44 and 3D7x31 correlation = -
268 0.12). As lower mean grey values correspond to higher amounts of melanin, these
269 correlations indicate that isolates that produce more melanin in a benign environment were
270 more tolerant to KCl stress, although this relationship was not significant at 8 dpi in the
271 3D7x3D1 cross.
272
273 **3.3. QTL results**
274 We identified at least one significant QTL for all but three traits (KCl melanisation rate, KCl
275 mean grey value at 12 dpi) in the 1A5x1E4 cross and all but one trait (KCl-tolerance affecting
276 melanisation rate) in the 3D7x3D1 cross (Table 1, for plots of all QTLs see Supplementary
277 Material S2 and S3). In general, the traits lacking significant QTLs had relatively low
278 heritability (Table 1) and thus the power to detect a QTL for those traits was relatively low.
279 All QTL positions, interval sizes and numbers of genes within the interval are presented in
280 Tables 2 and 3. Overlapping QTLs were grouped and given a unique QTL identifier. As
281 expected, traits that were highly correlated and/or statistically coupled often had a QTL
282 peak at the same, or overlapping positions (e.g. the 1A5x1E4 grey values in the control
283 environment at 8 dpi and 12 dpi mapped to the same position on Chr 2: 1438934bp; the
284 3D7x3D1 QTL for radius at 12 dpi and growth rate in the control environment mapped to
285 Chr 8: 1100862bp).
286
287 **3.4. QTLs shared across environments, traits, and time points**
288 Several QTLs were shared amongst benign and salt-stress environments, across time points
289 and traits. Only one of these shared QTLs is novel to this study, the other shared QTLs were
290 found in earlier studies investigating different stressors. The single novel QTL shared

291 between benign and salt-stress environments was found in the 3D7x3D1 cross on Chr 8
292 (1100.86-1221.33 Kb, QTL No. 9) and explained variation in seven traits including growth in
293 the control and KCl environments, as well as mean grey value in the control environment
294 and KCl tolerance at 8 dpi (Figure 1, Table 2).
295
296 Of the QTLs shared across benign and KCl environments that were identified here and found
297 in earlier studies using different stresses (e.g. cold, fungicide), the most striking – in terms of
298 the number of traits and the magnitude of the LODs, was the QTL on Chr 11 between
299 507.36-658.11 Kb (QTL No. 12) in the 3D7x3D1 cross. This QTL explained variation in 11 of
300 the 18 traits, and in both environments (Table 2). This QTL was identified previously and was
301 found to explain variation in growth, fungicide sensitivity and melanisation in this cross
302 (Lendenmann et al., 2015, 2014). The next largest, in terms of number of traits, was a QTL in
303 the 1A5x1E4 cross on Chr 8 (274.792- 346.224 Kb) that explained variation in growth rate in
304 both control and KCl environments and mean grey value in the control environment (Figure
305 2, Table 3). This QTL on Chr 8 was also found to explain variation in response to oxidative
306 stress (Zhong et al., 2021). Another notable QTL in terms of high LOD (>10) was on Chr 10
307 (775.47 – 924.42 Kb, QTL No. 10) in the 3D7x3D1 cross, which explained variation in
308 melanisation rate and colony radius in the control (Table 2). This QTL was previously found
309 to explain variation in growth-related traits at 10^0C (Lendenmann et al., 2014) and under
310 oxidative stress (Zhong et al., 2021).
311
312 **3.5. Unique QTLs associated with the KCl environment**
313 Several novel QTLs that were unique to the KCl environment were also found (Table 2, 3). In
314 the 3D7x3D1 cross, two QTLs were found for traits related to colony radius: the first on Chr
315 3 (QTL No. 3) explained variation in colony radius at 8 dpi and KCl-tolerance affecting colony
316 radius at 8 and 12 dpi; and the second on Chr 4 (QTL No. 5) explained variation in colony
317 radius at 8 dpi and KCl-tolerance affecting colony radius at 8 dpi. For melanin-related traits,
318 four QTLs were found in the 3D7x3D1 cross: the first on Chr 1 (QTL No. 1) explained
319 variation in three traits (melanisation rate, KCl-tolerance affecting melanisation rate and
320 grey value at 12 dpi); the second on Chr 2 (QTL No. 2) explained variation in grey value at 12
321 dpi; the third on Chr 6 (QTL No. 6) explained variation in melanisation rate; and the fourth
322 on Chr 8 (QTL No. 8) explained variation in grey value at 8 dpi. In the 1A5x1E4 cross a total

323 of six QTLs related to colony radius were found. The first three were on Chr 1: QTL No. 2
324 explained variation in KCl-tolerance affecting colony radius at 12 dpi; QTL No. 3 explained
325 variation in KCl-tolerance affecting growth rate; and QTL No. 4 explained variation in colony
326 radius at 12 dpi. The fourth unique KCl environment QTL Chr 5 (QTL No. 5) explained
327 variation in KCl-tolerance affecting growth rate; the fifth on Chr 6 (QTL No. 11) explained
328 variation in radius at 8 dpi; and the sixth on Chr 8 (QTL No. 14) explained variation in KCl-
329 tolerance affecting colony radius at 8 dpi. One QTL unique to the KCl environment was
330 found on Chr 8 (QTL No. 15) that explained variation in both radius- and melanin-related
331 traits, specifically KCl-tolerance affecting colony radius and grey value at 8 dpi.
332
333 To identify candidate genes associated with KCl stress, we focused attention on novel QTLs
334 with a high LOD (>10), relatively narrow intervals, and that explained a relatively high
335 proportion of the variation for a KCl-associated trait. Only QTL No. 3 in the 3D7x3D1 cross
336 met these requirements (Table 2). This QTL had a high LOD (>10) for colony radius at 8 dpi in
337 the KCl environment and KCl-tolerance affecting the radius at 8 dpi. The LOD peaked at 22.8
338 at chromosome position 737773 bp. This QTL explained 33% of the phenotypic variance in
339 colony radius at 8 dpi and 23% of the variance in KCl-tolerance affecting the radius at 8 dpi.
340 Isolates that had the non-reference allele at the LOD peak marker (X3_737773) were smaller
341 (F=113.1, df=1,233, p=<0.001, Figure 3c) and less KCl-tolerance affecting the radius at 8 dpi
342 (F=113.1, df=1,233, p=<0.001, Figure 3d). The Bayes confidence interval of this QTL spanned
343 163 Kb and contained 105 SNPs and 36 genes (Table 2, Figure 3b). For this interval we
344 present data on the genes in the reference genome (3D7), the orthologous genes in 3D1,
345 the gene sequence similarity (including ±200bp of flanking regions) between the parents,
346 the gene's putative encoded function (PFAM database) and if there is any evidence of
347 differential gene expression between the parents across all available datasets (Table 4 and
348 see Table S4 for full details).
349
350 **3.6. Candidate genes within QTL No. 3 in 3D7x3D1**
351 Several genes had SNP variation predicted to have a high impact based on SNPEff analysis
352 (Table S5, *ZT3D7_G3622*, *ZT3D7_G3623*, *ZT3D7_G3624, ZT3D7_G3632, ZT3D7_G3633,*
353 *ZT3D7_G3635, ZT3D7_G3649*). A transposable element (6927bp) was found within 200bp of
354 *ZT3D7_G3623*, and one gene, *ZT3D7_G3649* is a singleton – with no orthologue present in

355 any of the other 18 *Z. tritici* reference genome sequences (Table S4). Based on predicted
356 protein function, and sequence and gene expression variation between the parents, we
357 consider six genes to be the most promising candidates for further analyses: *ZT3D7_G3622*,
358 *ZT3D7_G3635*, *ZT3D7_G3637*, *ZT3D7_G3639*, *ZT3D7_G3655* and *ZT3D7_G3658* (this order
359 reflects their relative positions on chromosome 3).
360
361 *ZT3D7_G3622* has a loss of function SNP (Chr 3:598092) in 3D1 that is predicted to cause a
362 loss of a predicted start codon. The gene contains a single exon, encodes a protein length of
363 550 amino acids (aa) and was predicted to contain a fungal-specific transcription factor
364 domain and Zn(2)-C6 fungal-type DNA-binding domain (Table 4). The orthologue in the 3D1
365 genome is *ZT3D1_G3567*. It encodes a longer protein (722 aa) and has two exons, the first
366 exon's product encodes a Zn(2)-C6 fungal-type DNA-binding domain and the second exon's
367 product is the same as that of *ZT3D7_G3622*. The predicted protein in 3D1 is the same as
368 the orthologue in IPO323 (*Mycgr3T108446*). Although we do have reads mapping to this
369 region, and when grown in vitro on MM this gene is downregulated in 3D1 compared to 3D7
370 (Table S4), our RNA sequence data does not clearly support gene models in either 3D1 or
371 3D7, there are no clear exon/intron boundaries. This suggests that the annotation of this
372 gene may require manual curation.
373
374 *ZT3D7_G3635* has a high impact SNP variant (Chr 3:681906) that is predicted to cause a
375 frameshift. The gene has 6 exons in 3D7 and encodes a protein length of 1078 aa. Based on
376 INTERPROSCAN and Ensemble Fungi, the protein has multiple predicted domains; the
377 largest is a protein kinase domain. The protein also contains a Serine/threonine-protein
378 kinase active site and the molecular function of the first GO term (GO:0004674) is protein
379 serine/threonine kinase activity – suggesting that this gene is likely to be involved in osmotic
380 stress response (Hohmann, 2002). The RNA sequence data supports the gene model. The
381 orthologue in 3D1 is *ZT3D1_G3580*, which has 3 exons and multiple predicted domains that
382 do not differ from those predicted for *ZT3D7_G3635*. The gene is up-regulated in vitro on
383 YSB and down-regulated in planta at 28d in 3D1 compared to 3D7 (Table S4).
384
385 *ZT3D7_G3637* has one exon, encodes a protein length of 1285 aa, and includes multiple
386 predicted domains including a DEAD/DEAH box helicase, which is involved in plant

387 responses to osmotic stress (Nguyen et al., 2018). The orthologue in 3D1 (*ZT3D1_G3583*)
388 encodes a similar protein as *ZT3D7_G3637* – has the same length and has the same
389 predicted domains. There are no high impact SNPs between the parents, but several
390 moderate and low impact variants were identified (Table S5). The RNA sequence data
391 supports the annotation, and the gene is down regulated in 3D1 in both YSB and MM (Table
392 S4).
393
394 *ZT3D7_G3639* has 4 exons in 3D7. The gene sequence similarity between 3D7 and 3D1 is
395 98.66% and there is an 8bp intronic deletion in 3D1. This gene belongs to the Major
396 Facilitator Superfamily (MFS) and encodes a protein length of 512 aa. According to the
397 Phobius analysis, the gene contains 12 transmembrane segments (Table S4). Proteins with
398 transmembrane activity and transmembrane segments are likely to play an important role
399 in sensing and regulating osmotic stress (Hohmann, 2002). The orthologue in 3D1 is
400 *ZT3D1_G3580*, which has the same number of exons, encodes the same protein length and
401 has the same predicted function. The RNA sequence data supports the gene model, and the
402 differential expression analysis found the gene is downregulated in planta at 12 and 14 days
403 in 3D1 compared to 3D7 (Table S4).
404
405 *ZT3D7_G3655* has one exon and encodes a protein length of 848 aa. The gene contains 10
406 transmembrane segments (Table S4) and encodes a voltage-gated chloride channel domain
407 – thus it is likely to be involved in osmotic stress responses. The gene sequence between the
408 parents is almost identical, but there is one moderate effect SNP within the gene (Table S5).
409 When grown in vitro on MM this gene is upregulated in 3D1 compared to 3D7. The RNA
410 sequence data supports the gene model annotation.
411
412 *ZT3D7_G3658* has four exons and encodes a protein length of 614 aa. Its orthologue in 3D1
413 (*ZT3D1_G3604*) has three exons and encodes 572 aa. The gene encodes a vacuolar protein
414 sorting-associated protein 17, Vps17. Vacuoles play an important role in osmotic stress
415 responses: their fission and fusion enable cells to maintain turgor pressure and regulate cell
416 volume (Richards et al., 2010). Comparison of the 3D1 gene sequence to the 3D1 genome
417 using BLAST revealed that the 3D7 gene sequence was identical, but the 3D1 orthologue
418 annotation is shorter and has only three exons. Our RNA sequence data supports the 3D1

419 annotation with only 3 exons, as there were no RNA sequence reads mapping to exon 1 of
420 the *ZT3D7_G36580*. This gene was downregulated in vitro in both MM and YSB in 3D1
421 compared to 3D7.
422
423 **4. Discussion**
424 We were able to map major effect loci affecting colony growth and melanisation in the
425 presence of potassium chloride in both crosses. We focussed on QTLs that were unique to
426 the KCl environment to identify candidate genes that are specific to osmotic stress – as
427 opposed to finding genes that may be more generally related to intrinsic growth or melanin
428 production. A QTL on Chr 3 in the 3D7x3D1 cross was the most promising for identifying
429 genes specifically associated with KCl stress. We highlighted the six most promising
430 candidate genes in this QTL based on their predicted encoded functions, sequence similarity
431 and transcriptional profiles. We also identified several QTLs shared across environments and
432 confirmed that several previously identified QTLs, which explained variation in growth and
433 melanisation across different environmental stressors (Table 2 and 3, e.g. 3D7x3D1 Chr 11
434 and 1A5x1E4 Chr 8), also explained trait variation in the presence of osmotic stress.
435
436 **4.1. KCl tolerance**
437 In the presence of potassium chloride at 0.75M, colonies were typically smaller and less
438 melanised compared to the control environment (Table S1). A reduction in colony radius in
439 the KCl environment supports our hypothesis that this environment was stressful to *Z. tritici*.
440 Our results suggest that growth rate in the 1A5x1E4 cross was less affected by KCl-induced
441 osmotic stress, as mean growth rate was not reduced in the KCl environment, compared to
442 the 3D7x3D1 cross that exhibited a significantly reduced growth rate (Table S1). However,
443 we note that the overall difference in growth rate in the 3D7x3D1 progeny between the
444 control and KCl environments was relatively small (~6% reduction in growth, Table S1).
445
446 When experiencing osmotic stress, an increase in melanin is thought to protect cells by
447 strengthening the fungal cell wall, but a reduced metabolic capacity under stress may limit
448 the ability of a cell to produce melanin. The mean colony grey values were higher, indicative
449 of lower levels of melanin, for strains grown in the KCl environment (Table S1). This suggests
450 that the *Z. tritici* response to osmotic stress did not involve an increased production of

451 melanin to protect the cells as was observed in halotolerant species (Kogej et al., 2007). We
452 did observe however, that isolates that were more melanised in the benign control
453 environment were more tolerant to salt stress – their growth rates were higher and their
454 reductions in melanisation were lower compared to isolates that were less melanised in the
455 control environment (Table S2, S3). This suggests that strains having a greater intrinsic
456 capacity to become melanised are more tolerant to salt stress.
457
458 **4.2. Shared QTLs**
459 Some QTLs that explained variation in growth and melanisation in the stressful environment
460 overlapped with QTLs for trait variation in the control environment. Prominent examples
461 include the Chr 11 QTL at position 616039 in the 3D7x3D1 cross and the Chr 8 QTL at
462 position 274792- 346224 in the 1A5x1E4 cross. These genomic regions may harbour genes
463 that affect intrinsic growth of colonies under a wide range of environments and/or genes
464 with pleiotropic effects. Many of the QTLs shared across environments were identified in
465 earlier experiments and discussed previously (Lendenmann et al., 2015; Zhong et al., 2021).
466 The QTL on Chr 11 at position 616039 was shown to be due to differential expression of the
467 *Zmr1* gene encoding a transcription factor that regulates synthesis of DHN melanin in *Z.*
468 *tritici* (Krishnan et al. 2018). *Zmr1* was shown to have pleiotropic effects on melanin
469 production, colony growth rates and fungicide resistance (Krishnan et al. 2018).
470
471 **4.3. QTLs uniquely associated with the KCl environment**
472 This QTL analysis enabled us to identity large effect loci that explain variation in traits under
473 KCl stress. Among the QTLs uniquely associated with KCl stress, most had moderate LODs
474 with each QTL explaining only a small proportion of the phenotypic variance (3D7x3D1
475 maximum = 0.10, 1A5x1E4 maximum = 0.11). The exception was QTL No. 3 in the 3D7x3D1
476 cross, which explained up to 33% of the phenotypic variance. This QTL on chromosome 3
477 was associated with differences in radius at 8 dpi and KCl-tolerance affecting radius at 8 and
478 12 dpi. We targeted this QTL for further investigation seeking to identify genes specifically
479 associated with KCl tolerance. It is interesting to note that no LOD peak was detected for
480 colony radius at 12 dpi, even though radius at 12 dpi was correlated with radius at 8 dpi
481 (Table S2, correlation = 0.58, $p<0.001$). As growth rate is based on the change in radius
482 between 8 and 12 dpi, we might expect growth rate in KCl to share the QTL for colony size

483 at 8 dpi. To better understand why growth rate does not share this QTL, we examined the
484 trait correlations. Growth rate is highly correlated with colony radius at 12 dpi (0.93) and
485 less strongly correlated with colony radius at 8 dpi (0.26) (Table S2). There is less variation in
486 colony radius at 8 dpi, thus colony radius at 12 dpi has a greater impact on the growth rate.
487 The QTL also explained variation in KCl-tolerance affecting the radius at 8 and 12 dpi,
488 although the association with KCl-tolerance affecting the radius at 12 dpi explained
489 relatively little phenotypic variation (0.08). Thus, the QTL peak is more strongly associated
490 with radius and tolerance differences at an earlier stage of colony growth. A similar pattern
491 was observed in the chromosome 11 QTL associated with melanisation (Krishnan et al.,
492 2018; Lendenmann et al., 2014), with the QTL LOD score very high in the younger colonies
493 and decreasing as colonies aged. After cloning and characterizing the *Zmr1* gene and its
494 functions, this pattern could be explained based on the finding that the difference in *Zmr1*
495 expression (and the resulting difference in melanisation) was significantly higher in younger
496 colonies than in older colonies (Krishnan et al., 2018). We hypothesize that QTL no. 3
497 associated with KCl tolerance is underpinned by a similar mechanism that is specific to the
498 earlier stage of colony growth.
499
500 **4.4. Candidate genes in the QTL for radius and KCl-tolerance in radius at 8 dpi in the**
501 **3D7x3D1 cross**
502 Among the 36 genes found in the interval spanning this QTL on chromosome 3, we consider
503 six genes to be the most promising candidates to be involved in sensing and responding to
504 salt stress and responsible for this QTL. Below we consider each in turn in the order of their
505 relative positions on chromosome 3.
506
507 The first candidate gene, *ZT3D7_G3622*, is predicted to encode a fungal-specific
508 transcription factor. The orthologue in the IPO323 reference genome (assembly MYCGR
509 v2.0) is *Mycgr3T108446* and it has 21 paralogs. Transcription factors (TFs) regulate gene
510 expression and are important regulators of molecular responses to environmental stimuli
511 (e.g. Hohmann, 2002; Shi et al., 2021), making this gene a good candidate. The *Zmr1* gene
512 identified in this same cross and shown to be responsible for differences in melanisation,
513 with greater effects in younger colonies, is a transcription factor (Krishnan et al. 2018). The
514 SNP variant in 3D1 (Chr 3:598092) is predicted to cause a loss of the start codon that is likely

515 to cause a loss of function. In line with this, the mean radius of isolates carrying the 3D1
516 allele was smaller than the isolates carrying the 3D7 allele. In *F. graminearum* mutants
517 lacking a similar TF (called *Fss1*) were sensitive to high sodium and lithium, but they were
518 not sensitive to elevated potassium (Son et al., 2015).
519

520 The second candidate, *ZT3D7_G3635* is predicted to encode a serine/threonine-protein
521 kinase active site, which is known to regulate MAP kinases (Hohmann, 2002; Li et al., 2019).
522 A SNP variant found in the 3D1 allele is predicted to cause a frameshift that is likely to cause
523 a loss of function. The ortholog in the IPO323 genome is *Mycgr3G56270* and it has one
524 paralog in the reference genome. A serine/threonine kinase from *Aspergillus flavus*,
525 *AflSte20*, was recently functionally validated using a knockout mutant. This study showed
526 that the knockout had higher sensitivity to osmotic stress compared to the wild type (Li et
527 al., 2019), confirming the role of this serine/threonine-protein kinase in osmotic stress
528 response in a different fungal plant pathogen.
529

530 The third candidate, *ZT3D7_G3637* is predicted to encode a DEAD/DEAH box helicase
531 domain. The reference genome orthologue is *Mycgr3G99415* and it has 6 paralogs. The
532 DEAD – box helicases are the largest RNA helicase (RH) subfamily. In plants they play
533 multiple functional roles and are important in stress responses (Pandey et al., 2020). For
534 example, in *Arabidopsis thaliana AtRH17* is involved in salt-stress tolerance (Nguyen et al.,
535 2018), in rice *OsABP* is upregulated in response to salt (Macovei et al., 2012) and in barley
536 HvD1 accumulated in salt- and cold-stressed plants (Nakamura et al., 2004). In wheat, the
537 DEAD-box helicase *TaRH1* that was first identified as a component of the defence response
538 to stripe rust (*Puccinia striiformis f*. sp. *tritici*) was also found to be involved in plant
539 response to multiple stressors, including salt stress (Zhang et al., 2014). SNP variation found
540 between the parents was predicted to have only moderate effects, no high impact SNPs
541 were detected. We chose this gene as a promising candidate based mainly on its known
542 associations with salt stress in plants and the significant differences in expression found
543 between 3D1 and 3D7 while growing in vitro.
544

545 A gene encoding a Major Facilitator Superfamily (MFS) domain, *ZT3D7_G3639* is the fourth
546 candidate we highlight. The reference genome orthologue is *Mycgr3G85019* and it has 58
547 paralogs. MFS transporters facilitate the movement of small solutes across cell membranes
548 in response to chemiosmotic gradients – making them likely to play an important role in
549 sensing and regulating osmotic stress (Hohmann, 2002). We chose this gene as a promising
550 candidate based mainly on its known functions and associations with multiple stressors
551 including fungicides (Dos Santos et al., 2014; Omrane et al., 2015).
552

553 The fifth highlighted gene is *ZT3D7_G3655* that encodes a voltage gated chloride channel
554 domain and membrane transport domains. The reference genome orthologue is
555 *Mycgr3T20761* and there are three paralogues in the IPO323 reference genome. Chloride
556 channels are important in animal cell volume regulation (Jentsch et al., 2002), fungal
557 oxidative stress response (Oddon et al., 2007), fungal pathogen virulence (Cañero and
558 Roncero, 2008; Zhu and Williamson, 2003) and plant immunity (Guo et al., 2014). The role of
559 chloride channels in response to salt stress is well established in animals (Jentsch et al.,
560 2002), and to a lesser degree in plants (Barbier-Brygoo et al., 2011), but less is known from
561 fungi. For one of the better-known families of chloride channels, the CLC family, a single
562 gene (*GEF1*) has been identified in yeast. In two pathogenic fungi (*Cryptococcus neoformans*
563 and *Fusarium oxysporum*) – the GEF1 homologue has been shown to influence virulence
564 (Cañero and Roncero, 2008; Zhu and Williamson, 2003). The gene sequence between the
565 parents is highly conserved, however gene expression differences were observed in minimal
566 media, so differences may exist in the regulatory sequence.

567

568 The final candidate we highlight is *ZT3D7_G3658*, which encodes a Vacuolar associated
569 protein 17, *Vps17*. The orthologous gene in the reference genome is *Mycgr3T108464* and
570 there are six paralogues. Comparing the DNA sequence of this gene against the 3D1 genome
571 revealed an identical sequence, but the annotation of the 3D7 and 3D1 differs – the 3D1
572 orthologue protein length is shorter and the gene has one fewer exons. Our RNA sequence
573 data suggests that the *ZT3D7_G3658* annotation may be incorrect - there were no reads
574 mapping to the first, small exon of this gene. This suggests that the annotation of this gene

575 may need manual curation before conducting further analyses. The gene was
576 downregulated in YSB and MM in 3D1 compared to 3D7, demonstrating that transcription
577 of this gene varies between the parents. Vacuoles play important roles in both osmotic
578 stress responses (Richards et al., 2010) and virulence (Li et al., 2021). Under salt stress the
579 vacuoles can undergo fusion and fission – changing in size and number (Richards et al.,
580 2010). *Vsp17* knockouts in *S. cerevisiae* had many small vacuoles but were resistant to
581 osmotic stress and could sporulate (Köhrer and Emr, 1993). We are unaware of any work
582 that has investigated the role of *Vsp17* in salt-stress responses of filamentous fungi.
583
584
585 **4.5. QTL reproducibility**
586 This dataset allowed us to explore the repeatability of previously identified QTLs from other
587 published datasets. One earlier dataset used the same mapping populations but different
588 experimental conditions and treatments, with a different reference genome and different
589 genetic markers and map information (Lendenmann et al., 2015, 2014). A second earlier
590 dataset used the same isolates and experimental conditions, but different treatments and
591 different marker and map information (Zhong et al., 2021). Comparisons across these three
592 data sets yielded several consistent QTLs. Our analyses confirmed that a region on
593 chromosome 11 in the 3D7x3D1 cross (Table 2, QTL No. 11) is associated with variation in
594 melanisation and growth in multiple environments (e.g. under fungicide stress in
595 Lendenmann et al., 2015; under oxidative stress in Zhong et al., 2021). This QTL contains the
596 *Zmr1* transcription factor that was shown to regulate melanin production (Krishnan et al.,
597 2018). We hypothesize that *Zmr1* also explains the variation we observed under salt-stress.
598 A QTL associated with multiple growth and melanin traits in the 1A5x1E4 cross on
599 chromosome 8 (Table 3, QTL No. 13) overlaps with a previously identified QTL on
600 chromosome 8 that was associated with colony growth and tolerance to oxidative stress
601 (Zhong et al., 2021). These findings illustrate that many of our QTLs are reproducible across
602 experiments and increases our confidence that we have identified biologically meaningful
603 genomic regions using our automated image analyses.
604
605 **CRediT authorship contribution statement**

Jessica Stapley: Formal analysis, Data curation, Writing - Original Draft, Writing - Review & Editing, Resources, Data curation. Bruce A. McDonald: Conceptualization, Methodology, Writing - Review & Editing, Supervision, Project administration, Funding acquisition.

Declaration of Competing Interest

The authors declare that they have no known competing financial interests or personal relationships that could have appeared to influence the work reported in this paper

Data availability

Phenotypic and SNP data are available at ETH Data repository (DOI: 10.3929/ethz-b-000550424). All code and details of the analysis are available at (https://github.com/jessstapley/QTL-mapping-Z.-tritici).

Acknowledgments

We thank Ziming Zhong, Tiziana Valeria Vonlanthen, Bethan Turnbull, Susanne Dora, Sarah Furler, Alexandra Waltenspühl, and Jasmin Wiedmer for collecting the phenotypic data and Javier Palma-Guerrero for supervision. We thank Marcello Zala for assistance in the laboratory. This research was supported by the Swiss National Science Foundation (31003A_155955 granted to BAM).

627 **References**

628 Araújo, C.A.S., Ferreira, P.C., Pupin, B., Dias, L.P., Avalos, J., Edwards, J., Hallsworth, J.E.,
629 Rangel, D.E.N., 2020. Osmotolerance as a determinant of microbial ecology: A study
630 of phylogenetically diverse fungi. Fungal Biol. 124, 273–288.
631 https://doi.org/10.1016/j.funbio.2019.09.001
632 Badet, T., Oggenfuss, U., Abraham, L., McDonald, B.A., Croll, D., 2020. A 19-isolate
633 reference-quality global pangenome for the fungal wheat pathogen *Zymoseptoria*
634 *tritici*. BMC Biol. 18, 12. https://doi.org/10.1186/s12915-020-0744-3
635 Barbier-Brygoo, H., De Angeli, A., Filleur, S., Frachisse, J.-M., Gambale, F., Thomine, S.,
636 Wege, S., 2011. Anion channels/transporters in plants: from molecular bases to
637 regulatory networks. Annu. Rev. Plant Biol. 62, 25–51.
638 https://doi.org/10.1146/annurev-arplant-042110-103741
639 Broman, K.W., Wu, H., Sen, S., Churchill, G.A., 2003. R/qtl: QTL mapping in experimental
640 crosses. Bioinformatics 19, 889–890. https://doi.org/10.1093/bioinformatics/btg112
641 Cañero, D.C., Roncero, M.I.G., 2008. Influence of the chloride channel of *Fusarium*
642 *oxysporum* on extracellular laccase activity and virulence on tomato plants.
643 Microbiology 154, 1474–1481. https://doi.org/10.1099/mic.0.2007/015388-0
644 Croll, D., Zala, M., McDonald, B.A., 2013. Breakage-fusion-bridge Cycles and Large Insertions
645 Contribute to the Rapid Evolution of Accessory Chromosomes in a Fungal Pathogen.
646 PLOS Genet. 9, e1003567. https://doi.org/10.1371/journal.pgen.1003567
647 Dos Santos, S.C., Teixeira, M.C., Dias, P.J., Sá-Correia, I., 2014. MFS transporters required for
648 multidrug/multixenobiotic (MD/MX) resistance in the model yeast: understanding
649 their physiological function through post-genomic approaches. Front. Physiol. 5,
650 180–180. https://doi.org/10.3389/fphys.2014.00180
651 Duran, R., Cary, J.W., Calvo, A.M., 2010. Role of the Osmotic Stress Regulatory Pathway in
652 Morphogenesis and Secondary Metabolism in Filamentous Fungi. Toxins 2, 367–381.
653 https://doi.org/10.3390/toxins2040367
654 Francisco, C.S., Ma, X., Zwyssig, M.M., McDonald, B.A., Palma-Guerrero, J., 2019.
655 Morphological changes in response to environmental stresses in the fungal plant
656 pathogen *Zymoseptoria tritici*. Sci. Rep. 9, 9642. https://doi.org/10.1038/s41598-
657 019-45994-3
658 Francisco, C.S., McDonald, B.A., Palma-Guerrero, J., 2022. A transcription factor and a
659 phosphatase regulate temperature-dependent morphogenesis in a fungal plant
660 pathogen (preprint). Molecular Biology. https://doi.org/10.1101/2022.02.07.479299
661 Guo, W., Zuo, Z., Cheng, X., Sun, J., Li, H., Li, L., Qiu, J.-L., 2014. The chloride channel family
662 gene CLCd negatively regulates pathogen-associated molecular pattern (PAMP)-
663 triggered immunity in Arabidopsis. J. Exp. Bot. 65, 1205–1215.
664 https://doi.org/10.1093/jxb/ert484
665 Hohmann, S., 2002. Osmotic Stress Signaling and Osmoadaptation in Yeasts. Microbiol. Mol.
666 Biol. Rev. 66, 300–372. https://doi.org/10.1128/MMBR.66.2.300-372.2002
667 Jacob, S., Foster, A.J., Yemelin, A., Thines, E., 2015. High osmolarity glycerol (HOG) signalling
668 in *Magnaporthe oryzae*: Identification of MoYPD1 and its role in osmoregulation,
669 fungicide action, and pathogenicity. Fungal Biol. 119, 580–594.
670 https://doi.org/10.1016/j.funbio.2015.03.003
671 Jentsch, T.J., Stein, V., Weinreich, F., Zdebik, A.A., 2002. Molecular Structure and
672 Physiological Function of Chloride Channels. Physiol. Rev. 82, 503–568.
673 https://doi.org/10.1152/physrev.00029.2001

674 Jiang, C., Lv, G., Ge, J., He, B., Zhang, Z., Hu, Z., Zeng, B., 2021. Genome-wide identification
675 of the GATA transcription factor family and their expression patterns under
676 temperature and salt stress in *Aspergillus oryzae*. AMB Express 11, 56.
677 https://doi.org/10.1186/s13568-021-01212-w
678 Kogej, T., Stein, M., Volkmann, M., Gorbushina, A.A., Galinski, E.A., Gunde-Cimerman, N.,
679 2007. Osmotic adaptation of the halophilic fungus *Hortaea werneckii*: role of
680 osmolytes and melanization. Microbiology 153, 4261–4273.
681 https://doi.org/10.1099/mic.0.2007/010751-0
682 Köhrer, K., Emr, S., 1993. The yeast VPS17 gene encodes a membrane-associated protein
683 required for the sorting of soluble vacuolar hydrolases. J. Biol. Chem. 268, 559—569.
684 https://doi.org/10.1016/s0021-9258(18)54188-0
685 Krishnan, P., Meile, L., Plissonneau, C., Ma, X., Hartmann, F.E., Croll, D., McDonald, B.A.,
686 Sánchez-Vallet, A., 2018. Transposable element insertions shape gene regulation and
687 melanin production in a fungal pathogen of wheat. BMC Biol. 16, 78.
688 https://doi.org/10.1186/s12915-018-0543-2
689 Lendenmann, M.H., Croll, D., McDonald, B.A., 2015. QTL mapping of fungicide sensitivity
690 reveals novel genes and pleiotropy with melanization in the pathogen *Zymoseptoria*
691 *tritici*. Fungal Genet. Biol. 80, 53–67. https://doi.org/10.1016/j.fgb.2015.05.001
692 Lendenmann, M.H., Croll, D., Stewart, E.L., McDonald, B.A., 2014. Quantitative Trait Locus
693 Mapping of Melanization in the Plant Pathogenic Fungus *Zymoseptoria tritici*. G3
694 GenesGenomesGenetics 4, 2519–2533. https://doi.org/10.1534/g3.114.015289
695 Li, D., Qin, L., Wang, Y., Xie, Q., Li, N., Wang, S., Yuan, J., 2019. AflSte20 Regulates
696 Morphogenesis, Stress Response, and Aflatoxin Biosynthesis of *Aspergillus flavus*.
697 Toxins 11, 730. https://doi.org/10.3390/toxins11120730
698 Li, S., Zhang, S., Li, B., Li, H., 2021. The SNARE Protein CfVam7 Is Required for Growth,
699 Endoplasmic Reticulum Stress Response, and Pathogenicity of Colletotrichum
700 fructicola. Front. Microbiol. 12, 736066. https://doi.org/10.3389/fmicb.2021.736066
701 Liao, Y., Smyth, G.K., Shi, W., 2019. The R package Rsubread is easier, faster, cheaper and
702 better for alignment and quantification of RNA sequencing reads. Nucleic Acids Res.
703 47, e47–e47. https://doi.org/10.1093/nar/gkz114
704 Macovei, A., Vaid, N., Tula, S., Tuteja, N., 2012. A new DEAD-box helicase ATP-binding
705 protein (OsABP) from rice is responsive to abiotic stress. Plant Signal. Behav. 7,
706 1138–1143. https://doi.org/10.4161/psb.21343
707 Malosetti, M., van Eeuwijk, F.A., Boer, M.P., Casas, A.M., Elía, M., Moralejo, M., Bhat, P.R.,
708 Ramsay, L., Molina-Cano, J.-L., 2011. Gene and QTL detection in a three-way barley
709 cross under selection by a mixed model with kinship information using SNPs. Theor.
710 Appl. Genet. 122, 1605–1616. https://doi.org/10.1007/s00122-011-1558-z
711 Nakamura, T., Muramoto, Y., Yokota, S., Ueda, A., Takabe, T., 2004. Structural and
712 transcriptional characterization of a salt-responsive gene encoding putative ATP-
713 dependent RNA helicase in barley. Plant Sci. 167, 63–70.
714 https://doi.org/10.1016/j.plantsci.2004.03.001
715 Nguyen, L., Seok, H.-Y., Woo, D.-H., Lee, S.-Y., Moon, Y.-H., 2018. Overexpression of the
716 DEAD-Box RNA Helicase Gene AtRH17 Confers Tolerance to Salt Stress in
717 Arabidopsis. Int. J. Mol. Sci. 19, 3777. https://doi.org/10.3390/ijms19123777
718 Oddon, D.M., Diatloff, E., Roberts, S.K., 2007. A CLC chloride channel plays an essential role
719 in copper homeostasis in *Aspergillus nidulans* at increased extracellular copper

720 concentrations. Biochim. Biophys. Acta BBA - Biomembr. 1768, 2466–2477.
721 https://doi.org/10.1016/j.bbamem.2007.05.022
722 Omrane, S., Sghyer, H., Audéon, C., Lanen, C., Duplaix, C., Walker, A.-S., Fillinger, S., 2015.
723 Fungicide efflux and the MgMFS1 transporter contribute to the multidrug resistance
724 phenotype in *Z ymoseptoria tritici* field isolates: Fungicide efflux & *MgMFS 1*
725 contribute to MDR in *Z. tritici*. Environ. Microbiol. 17, 2805–2823.
726 https://doi.org/10.1111/1462-2920.12781
727 Palma-Guerrero, J., Ma, X., Torriani, S.F.F., Zala, M., Francisco, C.S., Hartmann, F.E., Croll, D.,
728 McDonald, B.A., 2017. Comparative Transcriptome Analyses in *Zymoseptoria tritici*
729 Reveal Significant Differences in Gene Expression Among Strains During Plant
730 Infection. Mol. Plant-Microbe Interactions® 30, 231–244.
731 https://doi.org/10.1094/MPMI-07-16-0146-R
732 Pandey, S., Prasad, A., Sharma, N., Prasad, M., 2020. Linking the plant stress responses with
733 RNA helicases. Plant Sci. 299, 110607.
734 https://doi.org/10.1016/j.plantsci.2020.110607
735 Plissonneau, C., Hartmann, F.E., Croll, D., 2018. Pangenome analyses of the wheat pathogen
736 *Zymoseptoria tritici* reveal the structural basis of a highly plastic eukaryotic genome.
737 BMC Biol. 16, 5. https://doi.org/10.1186/s12915-017-0457-4
738 Plissonneau, C., Stürchler, A., Croll, D., 2016. The Evolution of Orphan Regions in Genomes
739 of a Fungal Pathogen of Wheat. mBio 7. https://doi.org/10.1128/mBio.01231-16
740 R Core Team, 2020. R: A language and environment for statistical computing. R Foundation
741 for Statistical Computing, Vienna, Austria.
742 Richards, A., Veses, V., Gow, N.A.R., 2010. Vacuole dynamics in fungi. Fungal Biol. Rev. 24,
743 93–105. https://doi.org/10.1016/j.fbr.2010.04.002
744 Robinson, M.D., McCarthy, D.J., Smyth, G.K., 2010. edgeR: a Bioconductor package for
745 differential expression analysis of digital gene expression data. Bioinformatics 26,
746 139–140. https://doi.org/10.1093/bioinformatics/btp616
747 RStudio Team, 2020. RStudio: Integrated Development Environment for R. RStudio, Boston,
748 MA.
749 Shi, D., Ren, W., Wang, J., Zhang, J., Mbadianya, J.I., Mao, X., Chen, C., 2021. The
750 transcription factor FgNsf1 regulates fungal development, virulence and stress
751 responses in Fusarium graminearum. J. Integr. Agric. 20, 2156–2169.
752 https://doi.org/10.1016/S2095-3119(20)63339-1
753 Son, H., Park, A.R., Lim, J.Y., Lee, Y.-W., 2015. Fss1 is involved in the regulation of an *ENA5*
754 homologue for sodium and lithium tolerance in *F usarium graminearum*: Roles of
755 Fss1 in *Fusarium graminearum*. Environ. Microbiol. 17, 2048–2063.
756 https://doi.org/10.1111/1462-2920.12757
757 Zhang, X., Zhao, X., Feng, C., Liu, N., Feng, H., Wang, X., Mu, X., Huang, L., Kang, Z., 2014. The
758 cloning and characterization of a DEAD-Box RNA helicase from stress-responsive
759 wheat. Physiol. Mol. Plant Pathol. 88, 36–42.
760 https://doi.org/10.1016/j.pmpp.2014.07.004
761 Zhong, Z., Marcel, T.C., Hartmann, F.E., Ma, X., Plissonneau, C., Zala, M., Ducasse, A.,
762 Confais, J., Compain, J., Lapalu, N., Amselem, J., McDonald, B.A., Croll, D., Palma-
763 Guerrero, J., 2017. A small secreted protein in *Zymoseptoria tritici* is responsible for
764 avirulence on wheat cultivars carrying the Stb6 resistance gene. New Phytol. 214,
765 619–631. https://doi.org/10.1111/nph.14434

766 Zhong, Z., McDonald, B.A., Palma-Guerrero, J., 2021. Tolerance to oxidative stress is
767 associated with both oxidative stress response and inherent growth in a fungal
768 wheat pathogen. Genetics 217, iyaa022. https://doi.org/10.1093/genetics/iyaa022
769 Zhu, X., Williamson, P.R., 2003. A CLC-type chloride channel gene is required for laccase
770 activity and virulence in *Cryptococcus neoformans*: CLC-A of *Cryptococcus*
771 *neoformans*. Mol. Microbiol. 50, 1271–1281. https://doi.org/10.1046/j.1365-
772 2958.2003.03752.x
773

774

775 **Figure 1.** Genome scan from the 3D7x3D1 cross of a) growth rate and b) melanisation rate
776 in the control (grey) and in the KCl environment (orange). The dashed horizontal lines
777 indicate the LOD significance thresholds for each trait based on permutation.
778
779 **Figure 2**. Genome scan from the 1A5x1E4 cross of a) growth rate and b) melanisation rate in
780 the control (grey) and in the KCl environment (orange). The dashed horizontal lines indicate
781 the LOD significance thresholds for each trait based on permutation.
782
783 **Figure 3.** QTL interval on Chromosome 3 for colony radius at 8 dpi in the 3D7x3D1 cross. a)
784 LOD peak and Bayes credible interval (shaded) with SNP positions indicated on the x-axis as
785 black vertical lines, b) Alignment of the genes within the QTL interval between the 3D7 and
786 3D1 parental strains – orange-coloured genes are the six most promising candidate genes
787 described in the main text and c) allelic effect of the SNP with the highest LOD on colony
788 radius at 8 dpi and d) allelic effect of the SNP with the highest LOD on KCl-tolerance
789 affecting colony radius at 8 dpi.
790
791
792 Supplementary Material
793 S1. Summary of genetic linkage maps.
794 S2. Genome scans from the 3D7x3D1 cross for all traits.
795 S3. Genome scans from the 1A5x1E4 cross for all traits.
796
797
798

Table 1. Summary of the QTL mapping results for all traits. The details of each trait are as follows, data type indicates if the measurement was made at a single time point (days post inoculation, DPI) or if it was calculated across two time points (Rate) or across two environments (Tolerance) (see Methods for details). The environment indicates the treatment conditions the colonies were grown in, control, potassium chloride (KCl), or calculated as a ratio across both environments (both). The measurement column indicates if the measurement was colony radius, grey value (indicator of melanin) or the change in radius or melanin over time (growth rate, melanisation rate). For example, row 1: colony radius measured at 8 DPI in the control environment. The QTL peak columns show the chromosomal position of significant QTL peak for each trait in the 3D7x3D1 and 1A5x1E4 crosses respectively, and the final column contained estimated heritability (h^2) for each trait.

Data Type	**Environment**	**DPI**	**Measurement**	**QTL peak 3D7x3D1**	**h^2**	**QTL peak 1A5x1E4**	**h^2**
Time point	Control	8	Radius	3,8,10,11	0.53	2,3,8	0.56
Time point	Control	12	Radius	3,7,8,10,11	0.62	7,8	0.48
Time point	KCl	8	Radius	3,4	0.64	6,	0.50
Time point	KCl	12	Radius	3,8	0.60	1,8	0.52
Time point	Control	8	Grey value	8,10,11	0.42	1,2,3,8	0.63
Time point	Control	12	Grey value	11	0.22	2,3,8	0.44
Time point	KCl	8	Grey value	8,11	0.54	8	0.34
Time point	KCl	12	Grey value	1,2,11	0.34	No Sig. QTL	0.29
Rate	Control	8-12	Growth rate	3,8,11	0.61	7,8	0.33
Rate	KCl	8-12	Growth rate	3,8,11	0.45	8,	0.49
Rate	Control	8-12	Melanisation rate	10	0.28	2,3,12	0.54
Rate	KCl	8-12	Melanisation rate	1,6	0.32	No Sig. QTL	0.27
Tolerance	Both	8	Grey value	8,10	0.37	1,2,3,8	0.58
Tolerance	Both	12	Grey value	11	0.18	No Sig. QTL	0.34
Tolerance	Both	8	Radius	3,4,10	0.59	8	0.42
Tolerance	Both	12	Radius	3,10,11	0.47	1	0.37
Tolerance	Both	8-12	Growth rate	11	0.40	1,5	0.45
Tolerance	Both	8-12	Melanisation rate	No Sig. QTL	0.14	1	0.32

Table 2. Description of all QTLs identified from the 3D7x3D1 cross, including map and physical position of the LOD peak marker, the bayes credible interval length and the number of genes within the interval. PVE is the proportion of variance explained by the QTL. QTL number is a number assigned to a particular QTL peak which identifies overlapping QTLs.

Type	Measurement	Environment	DPI	Chr	Pos (cM)	LOD	Pos (bp)	No. markers	Interval Start (bp)	Interval end (bp)	Interval size (bp)	No. Genes	PVE	QTL number
Rate	Melanisation rate	KCl	8-12	1	457.43	6.18	1590235	2915	1035571	2769729	1734.158	598	0.10	1
Tolerance	Melanisation rate	Ratio	8-12	1	540.00	3.40	2295356	9000	788430	6389989	5601.559	1977	0.06	1
Time point	Grey value	KCl	12	1	576.00	5.99	2717234	519	2295128	2769729	474.601	174	0.10	1
Time point	Grey value	KCl	12	2	261.00	5.07	691536	141	679366	711981	32.615	15	0.09	2
Tolerance	Radius	Ratio	12	3	142.92	4.49	719549	553	396401	944712	548.311	125	0.08	3
Tolerance	Radius	Ratio	8	3	144.00	14.62	737773	105	588483	751983	163.5	36	0.23	3
Time point	Radius	KCl	8	3	144.15	22.83	737773	94	588483	737773	149.29	31	0.33	3
Rate	Growth rate	Control	8-12	3	415.00	5.31	2537296	2204	1982744	3347765	1365.021	462	0.09	4
Time point	Radius	Control	12	3	456.63	8.11	2993469	427	2971359	3196103	224.744	79	0.13	4
Time point	Radius	Control	8	3	482.67	7.09	3056536	428	2982086	3199430	217.344	76	0.12	4
Time point	Radius	KCl	12	3	485.65	4.99	3110053	3084	516017	3203947	2687.93	813	0.08	4
Rate	Growth rate	KCl	8-12	3	485.65	4.93	3110053	845	2971359	3347765	376.406	132	0.08	4
Tolerance	Radius	Ratio	8	4	400.00	4.28	1936846	1000	1845763	2448166	602.403	200	0.07	5
Time point	Radius	KCl	8	4	403.76	4.37	2013908	986	1867509	2448166	580.657	194	0.07	5
Rate	Melanisation rate	KCl	8-12	6	220.14	6.24	1767543	479	1568163	1981193	413.03	124	0.10	6
Time point	Radius	Control	12	7	186.78	4.47	1109088	1366	511101	1377451	866.35	265	0.08	7
Time point	Grey value	KCl	8	8	680.87	5.69	943669	732	502305	974947	472.642	123	0.10	8
Time point	Radius	Control	12	8	746.72	10.77	1100862	274	1091579	1164224	72.645	29	0.17	9
Rate	Growth rate	Control	8-12	8	746.72	7.31	1100862	542	1071962	1221280	149.318	65	0.12	9
Rate	Growth rate	KCl	8-12	8	747.72	9.66	1100862	667	1091692	1284370	192.678	77	0.16	9
Time point	Radius	KCl	12	8	751.61	9.79	1112633	670	1100862	1292397	191.535	76	0.16	9
Time point	Radius	Control	8	8	765.72	8.04	1221337	751	1091475	1354349	262.874	108	0.13	9

Tolerance	Grey value	Ratio	8	8	776.11	4.22	1350673	2608	962119	2165894	1203.775	457	0.07	9
Time point	Grey value	Control	8	8	776.11	4.35	1350706	2549	981398	2175005	1193.607	450	0.07	9
Time point	Grey value	Control	8	10	199.98	12.37	775475	160	769669	861699	92.03	32	0.20	10
Tolerance	Grey value	Ratio	8	10	199.98	10.68	775475	281	769669	919978	150.309	56	0.17	10
Rate	Melanisation rate	KCl	8-12	10	200.35	8.66	792011	299	769669	924425	154.756	59	0.14	10
Time point	Radius	Control	8	10	200.72	12.32	792272	299	769669	924425	154.756	59	0.19	10
Tolerance	Radius	Ratio	8	10	211.51	10.58	924412	283	792019	924425	132.406	53	0.17	10
Tolerance	Radius	Ratio	12	10	211.51	6.68	924414	1081	749521	1302645	553.124	211	0.11	10
Time point	Radius	Control	12	10	212.61	4.92	924425	540	749521	1054575	305.054	116	0.08	10
Time point	Radius	Control	8	11	183.07	4.20	507361	528	311631	698718	387.087	128	0.07	11
Tolerance	Radius	Ratio	12	11	188.28	5.60	581439	1340	74200	890544	816.344	268	0.09	11
Time point	Grey value	KCl	12	11	192.28	6.87	605810	408	463714	776764	313.05	99	0.11	11
Time point	Radius	Control	12	11	193.00	16.79	616039	25	601600	658119	56.519	16	0.26	11
Rate	Growth rate	KCl	8-12	11	193.00	5.47	616039	219	468760	698718	229.958	72	0.09	11
Rate	Growth rate	Control	8-12	11	193.00	19.63	616039	5	616039	658119	42.08	13	0.29	11
Time point	Grey value	Control	12	11	194.11	6.64	657530	498	514049	870059	356.01	121	0.11	11
Tolerance	Grey value	Ratio	12	11	194.11	5.55	657530	700	367519	870059	502.54	168	0.09	11
Time point	Grey value	Control	8	11	194.11	5.30	658070	244	463714	704331	240.617	77	0.09	11
Time point	Grey value	KCl	8	11	194.11	17.09	658119	5	616039	658119	42.08	13	0.26	11
Tolerance	Growth rate	Ratio	8-12	11	195.28	7.45	658119	370	500942	802650	301.708	98	0.12	11

820 **Table 3**. Description of all QTLs identified from the 1A5x1E4 cross, including map and physical position of the LOD peak marker, the bayes
821 credible interval length and the number of genes within the interval. PVE is the proportion of variance explained by the QTL. QTL number is a
822 number assigned to a particular QTL peak which identifies overlapping QTLs..
823

Type	Measurement	Environment	DPI	Chr	Pos (cM)	LOD	Pos (bp)	No. markers	Interval Start (bp)	Interval end (bp)	Interval size (bp)	No. Genes	PVE	QTL number
Time point	Grey value	Control	8	1	328.91	5.69	572065	402	442697	727696	284.999	92	0.10	1
Tolerance	Melanisation rate	Ratio	8-12	1	328.91	4.46	572065	463	461577	779936	318.359	102	0.08	1
Tolerance	Grey value	Ratio	8	1	328.91	5.01	572065	405	442697	732023	289.326	93	0.08	1
Tolerance	Radius	Ratio	12	1	559.12	4.07	1849200	4654	399579	5725682	5326.103	1964	0.07	2
Tolerance	Growth rate	Ratio	8-12	1	797.00	4.80	3405315	3068	399544	3488556	3089.012	1151	0.08	3
Time point	Radius	KCl	12	1	1104.00	4.03	5792644	4774	372886	5956797	5583.911	2056	0.07	4
Rate	Grey value	Control	8-12	2	70.00	6.56	574965	1211	405115	1914465	1509.35	509	0.11	5
Time point	Grey value	Control	12	2	204.66	4.55	1438934	618	1284536	2152463	867.927	281	0.08	6
Time point	Grey value	Control	8	2	204.66	18.08	1438934	185	1438863	1748215	309.352	95	0.27	6
Tolerance	Grey value	Ratio	8	2	204.66	15.97	1438934	184	1438934	1748215	309.281	95	0.24	6
Time point	Radius	Control	8	2	211.42	8.76	1631840	217	1438934	1776132	337.198	105	0.14	6
Tolerance	Grey value	Ratio	8	3	147.00	6.15	1325440	210	1243932	1684531	440.599	179	0.10	7
Time point	Grey value	Control	8	3	148.00	6.66	1325440	133	1325422	1592801	267.379	115	0.11	7
Time point	Radius	Control	8	3	163.74	5.83	1521535	725	355042	1592801	1237.759	374	0.10	8
Rate	Grey value	Control	8-12	3	193.38	11.99	1711037	290	1489966	2105601	615.635	180	0.19	9
Time point	Grey value	Control	12	3	198.73	4.04	1928783	860	1743111	2927356	1184.245	361	0.07	9
Tolerance	Growth rate	Ratio	8-12	5	399.00	4.34	2638913	155	2511016	2658480	147.464	48	0.07	10
Time point	Radius	KCl	8	6	179.00	4.48	1512508	594	778583	1557528	778.945	256	0.08	11
Rate	Growth rate	Control	8-12	7	158.82	4.43	539824	255	437699	651318	213.619	80	0.07	12
Time point	Radius	Control	12	7	158.82	4.67	539837	254	437718	651318	213.6	80	0.08	12
Rate	Growth rate	KCl	8-12	8	76.80	8.79	274792	82	256529	346224	89.695	25	0.14	13
Time point	Radius	KCl	12	8	76.80	8.94	274792	67	256529	313758	57.229	17	0.15	13

Time point	Grey value	Control	12	8	78.58	4.92	302772	882	89684	921404	831.72	308	0.08	13
Time point	Radius	Control	12	8	79.00	9.72	302772	80	260355	346224	85.869	24	0.16	13
Time point	Grey value	Control	8	8	79.00	12.12	302772	66	270834	346224	75.39	22	0.19	13
Time point	Radius	Control	8	8	79.00	11.06	302772	415	260101	732444	472.343	163	0.18	13
Tolerance	Grey value	Ratio	8	8	79.00	8.26	302772	339	89573	346224	256.651	90	0.14	13
Tolerance	Radius	Ratio	8	8	137.00	5.05	832180	1177	589084	1648406	1059.322	396	0.08	14
Time point	Grey value	KCl	8	8	164.00	4.33	1377926	1406	305075	1623437	1318.362	485	0.07	14
Rate	Grey value	Control	8-12	12	126.74	4.24	473688	275	441706	821603	379.897	101	0.07	15

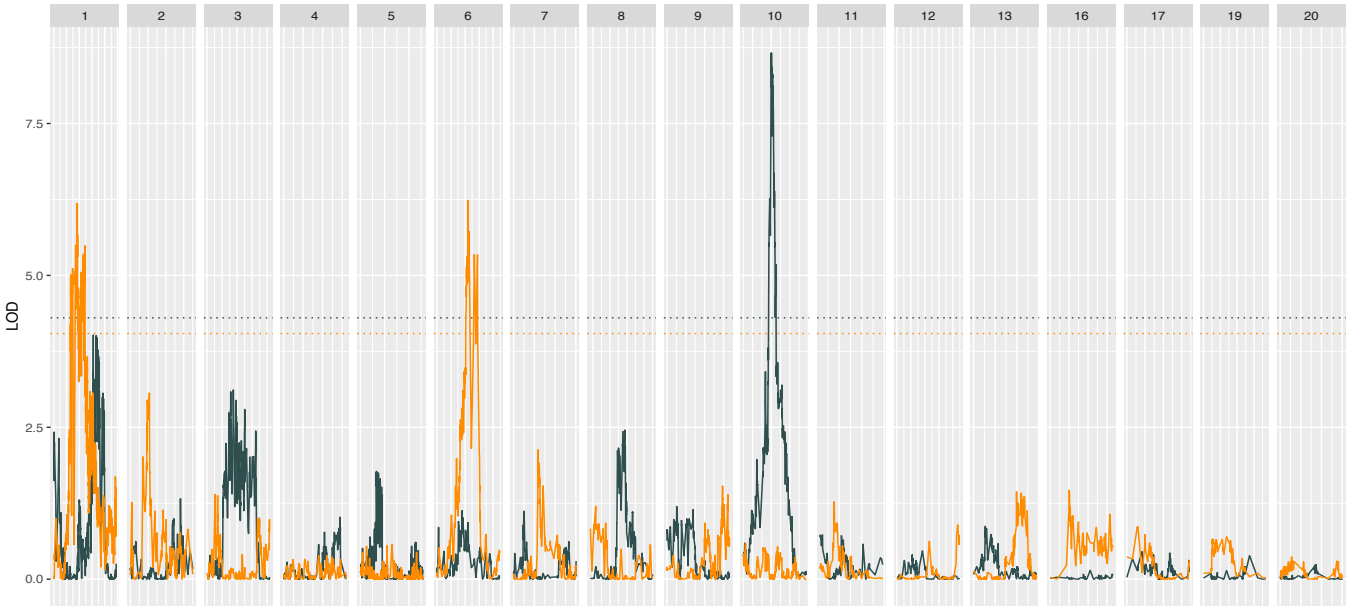

Growth rate — Control — KCl

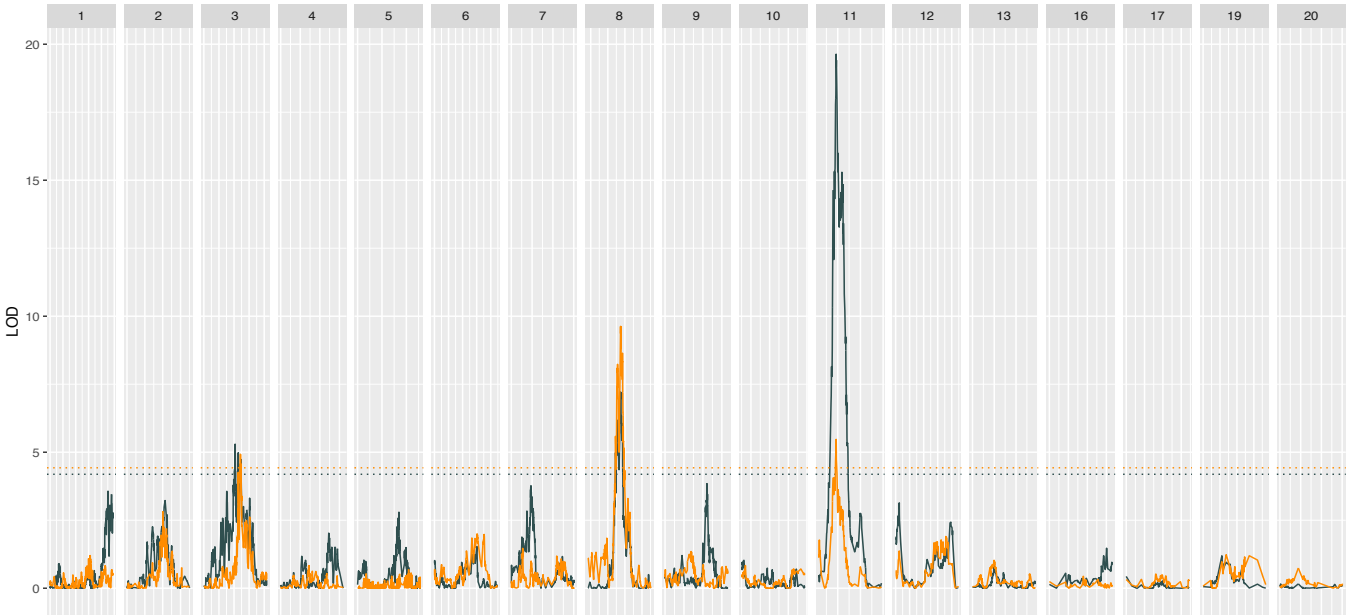

Melanisation rate — Control — KCl

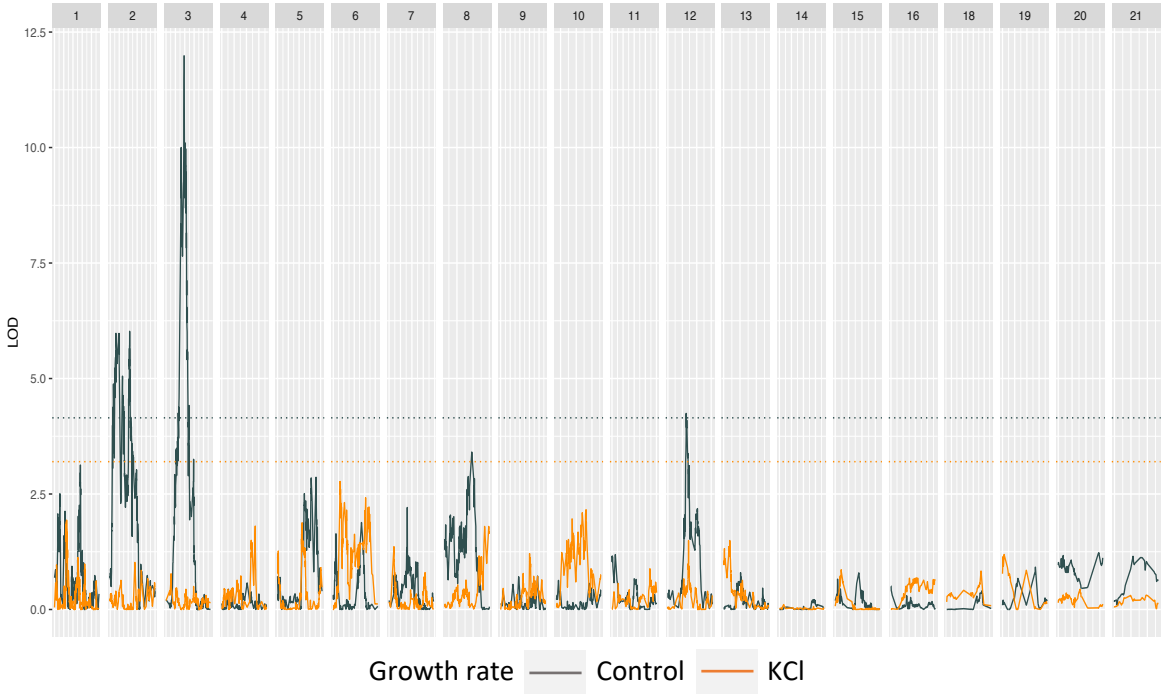
1
2
3
4
5
6
7
8
9
10
11
12
13
14
15
16
18
19
20
21
12.5
10.0
7.5
5.0
2.5
0.0
LOD
Growth rate
Control
KCl

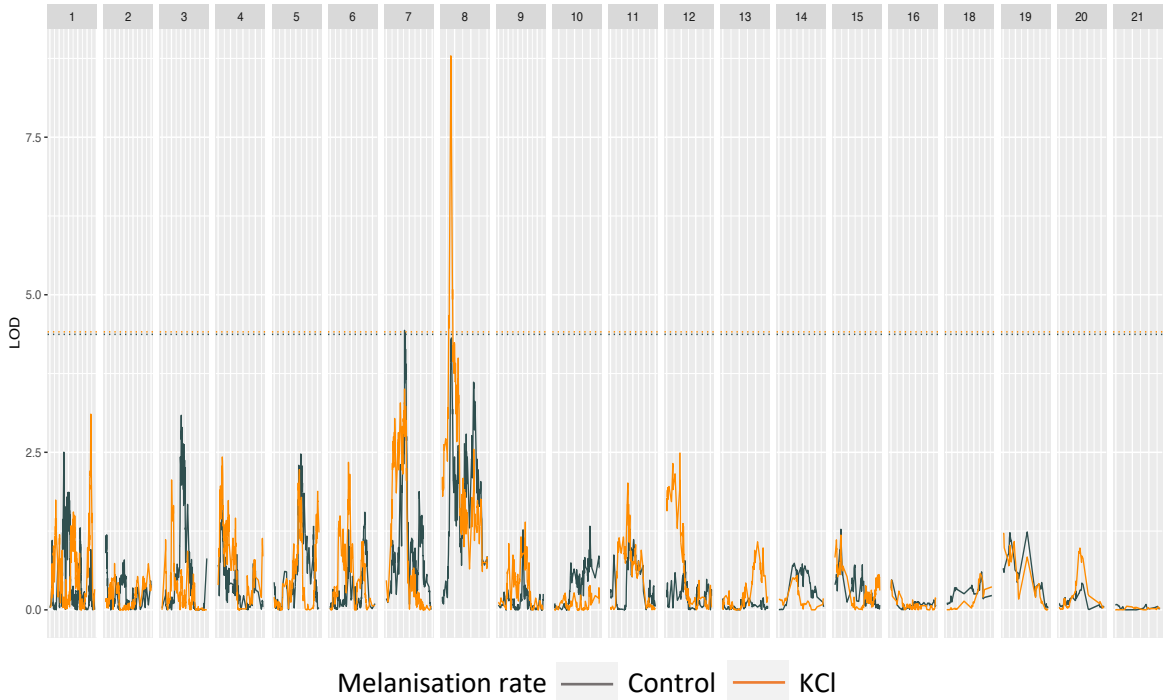
1
2
3
4
5
6
7
8
9
10
11
12
13
14
15
16
18
19
20
21
7.5
5.0
2.5
0.0
LOD
Melanisation rate
Control
KCl

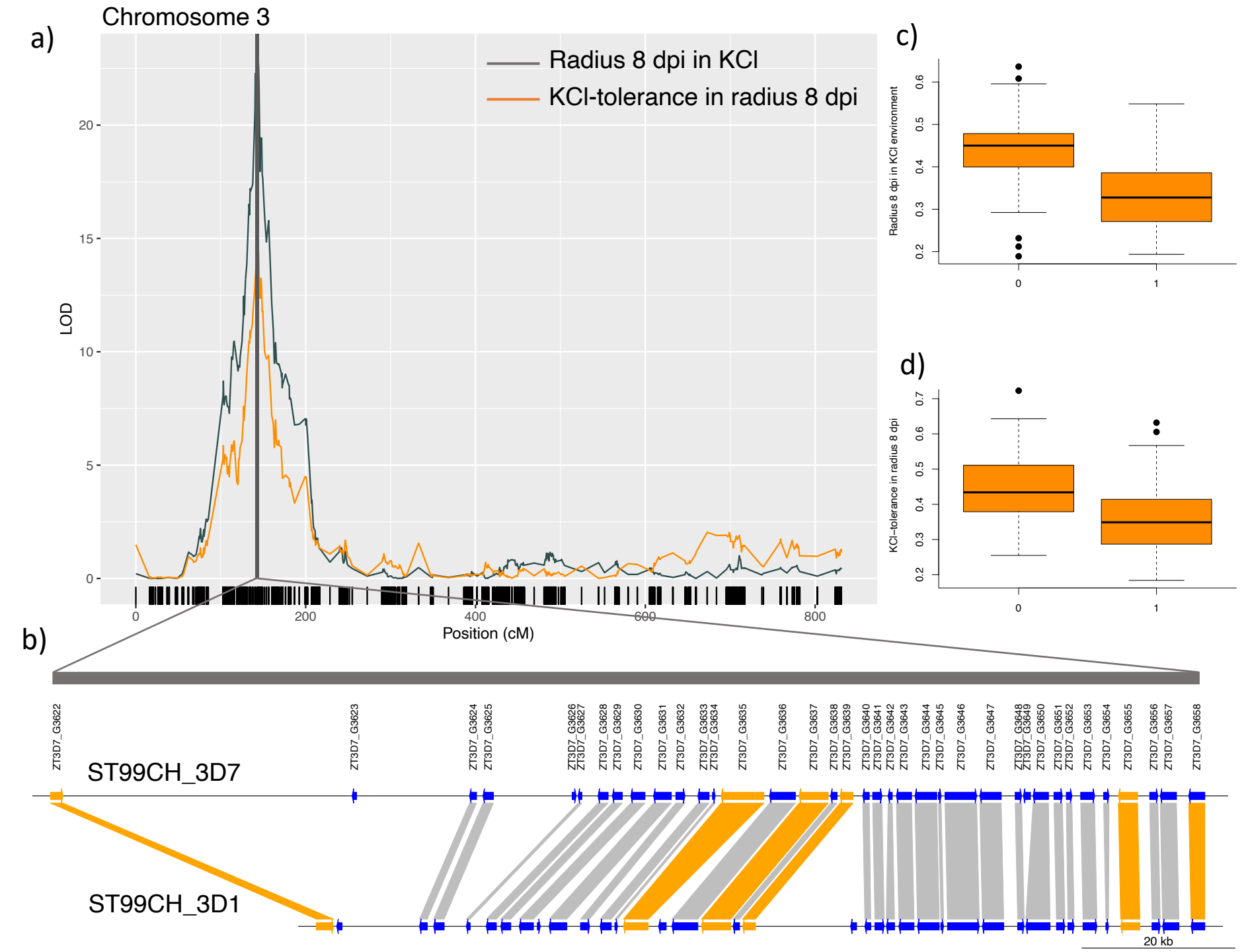
a)
Chromosome 3
Radius 8 dpi in KCl
KCl-tolerance in radius 8 dpi
LOD
Position (cM)
b)
ST99CH_3D7
ST99CH_3D1
20 kb
c)
Radius 8 dpi in KCl environment
d)
KCl−tolerance in radius 8 dpi